Residues 207, 216, and 221 and the Catalytic Activity of mGSTA1-1 and mGSTA2-2 toward Benzo[*a*]pyrene-(7*R*,8*S*)-diol-(9*S*,10*R*)-epoxide[†,‡]

Yijun Gu,[§,||] Bing Xiao,[§,⊥] Heather L. Wargo,[§,#] Matthew H. Bucher,[§,@] Shivendra V. Singh,[||] and Xinhua Ji*[,§]

Macromolecular Crystallographic Laboratory, National Cancer Institute, Frederick, Maryland 21702, and Department of Pharmacology and University of Pittsburgh Cancer Institute, University of Pittsburgh, Pittsburgh, Pennsylvania 15261

Received September 3, 2002; Revised Manuscript Received December 2, 2002

ABSTRACT: Murine class alpha glutathione *S*-transferase subunit types A2 (mGSTA2-2) and A1 (mGSTA1-1) have high catalytic efficiency for glutathione (GSH) conjugation of the ultimate carcinogenic metabolite of benzo[*a*]pyrene, (+)-*anti*-7,8-dihydroxy-9,10-oxy-7,8,9,10-tetrahydrobenzo[*a*]pyrene, [(+)-*anti*-BPDE]. Only 10 residues differ between the sequences of mGSTA1-1 and 2-2. However, the catalytic efficiency of mGSTA1-1 for GSH conjugation of (+)-*anti*-BPDE is >3-fold higher as compared with mGSTA2-2. The crystal structure of mGSTA1-1 in complex with the GSH conjugate of (+)-*anti*-7,8-dihydroxy-9,10-oxy-7,8,9,10-tetrahydrobenzo[*a*]pyrene (GSBpd) reveals that R216 and I221 in the last helix play important roles in catalysis [Gu, Y., Singh, S. V., and Ji, X. (2000) *Biochemistry 39*, 12552−12557]. The crystal structure of mGSTA2-2 in complex with GSBpd has been determined, which reveals a different binding mode of GSBpd. Comparison of the two structures suggests that residues 207 and 221 are responsible for the different binding mode of GSBpd and therefore contribute to the distinct catalytic efficiency of the two isozymes.

Glutathione *S*-transferases (GSTs[1], EC 2.5.1.18) catalyze the addition of glutathione (GSH) to xenobiotic substrates that have an electrophilic functional group. The catalytic diversity of this family of detoxification enzymes arises, in part, from the existence of at least 14 distinct gene classes: alpha, beta, delta, kappa, lambda, mu, omega, phi, pi, sigma, theta, tau, zeta, and microsomal GSTs (*1, 2*). Although GST isozymes of each class exhibit relatively broad substrate selectivity, most have unique catalytic attributes that are important in defining their physiological significance (*1*, *3*−*6*). The extent of understanding the precise enzyme−substrate interactions responsible for the catalytic properties has been greatly increased by the recent determinations of many three-dimensional structures of GSTs (*1*, *7*). Both the GSH-binding site (G-site) and the xenobiotic substrate-binding site (H-site) are defined by these crystal structures. The G-site is very well-defined for the cytosolic GSTs, and three different GSH-binding modes have been summarized by Ji et al. (*8*). In contrast, the binding modes of xenobiotic substrates and product molecules are much more complex and class specific. For example, the H-site in rGSTM1-1 is a hydrophobic cavity (*9*), whereas in hGSTP1-1 it is half-hydrophobic and half-hydrophilic with functionally important water molecules (*8*, *10*).

GSTs play an important role in the cellular defense against the carcinogenic effects of polycyclic hydrocarbons (PAHs), which are widespread environmental pollutants (*11*). The mutagenic and carcinogenic activities of many PAHs, including the prototypical member benzo[*a*]pyrene (BP), are attributed to their respective diol epoxides (*12*−*14*), which are substrates for GSTs (*15*−*19*). The GST isozymes of various classes differ remarkably in their activity toward PAH-diol epoxides (*15*−*19*). For example, previous studies with purified human and rat GST isozymes have shown that the class pi isozyme is relatively more efficient than other classes of GSTs in the GSH conjugation of (+)-*anti*-7,8-dihydroxy-9,10-oxy,7,8,9,10-tetrahydrobenzo[*a*]pyrene [(+)-*anti*-BPDE] (*15*, *16*), which is the ultimate carcinogenic metabolite of BP (*13*, *14*). These studies have also shown that (+)-*anti*-BPDE is a poor substrate for class alpha GSTs from rat and human (*15*−*17*). More recently, we have demonstrated that mGSTA1-1 and mGSTA2-2 are highly efficient alpha class GSTs in the GSH conjugation of (+)-*anti*-BPDE (*20*). The catalytic efficiency of mGSTA1-1 is approximately 3.3−655-fold higher than that of other murine GSTs, including mGSTA2-2, mGSTP1-1, mGSTA3-3, mGSTM1-1, or mGSTA4-4 (*20*−*22*).

[†] This work was supported in part by USPHS Grants R01 CA76348 and CA55589 (to S.V.S.).

[‡] The atomic coordinates and structure factors have been deposited with the Protein Data Bank under accession code 1ML6.

* Address correspondence to this author. Phone: (301) 846-5035; fax: (301) 846-6073; e-mail: jix@ncifcrf.gov.

[§] National Cancer Institute.

[||] University of Pittsburgh.

[⊥] Current address: National Institute for Medical Research, Mill Hill, London NW7 1AA, UK.

[#] Current address: HIV Drug Resistance Program, National Cancer Institute, Frederick, MD 21702.

[@] Current address: University of Virginia School of Medicine, Charlottesville, VA, 22908.

[1] Abbreviations: GSH, glutathione; GST, GSH *S*-transferase; xGSTY*m*-*n*, class Y (A, alpha; M, mu; P, pi; T, theta; S, sigma; K, kappa) GST with subunit type *m*-*n* (*m* and *n* = 1, 2 ...) from x (m, murine; h, human; r, rat; s, squid; b, bovine); BP, benzo[*a*]pyrene; (+)-*anti*-BPDE, (+)-*anti*-7,8-dihydroxy-9,10-oxy-7,8,9,10-tetrahydrobenzo[*a*]pyrene; GSBpd, GSH conjugate of (+)-*anti*-BPDE; G-site, GSH-binding site; H-site, xenobiotic substrate-binding site; PAH, polycyclic aromatic hydrocarbon; rms, root-mean-square.

10.1021/bi026778+ CCC: $25.00
Published on Web 01/07/2003

Table 1: Summary of Data Collection for MGSTA2-2·GSBpd

wavelength (Å)	0.92
space group	*C*2
crystal−detector distance (mm)	150
total frames collected	190
$\Delta\varphi$ (deg)	1.0
unit cell parameters	
a, *b*, *c* (Å)	99.07, 93.90, 52.60
β (deg)	92.28
resolution (Å)	30.0−1.9
redundancy	4.59
completeness (%): overall/ last shell[a]	99.7/99.2
$I/\sigma(I)$: overall/last shell[a]	18.68/2.44
R_{merge}[b]	0.062

[a] 1.97−1.90 Å. [b] $R_{merge} = \sum|I - \langle I\rangle|/\sum I$. Friedel pairs were merged.

Table 2: Summary of Refinement Statistics for MGSTA2-2·GSBpd

resolution range (Å)	30.0−1.9
number of reflections with $I/\sigma(I) \geq 0$	37 774
working set for refinement	35 892
test set for R_{free} calculation	1882
R-factor (%)[a]	20.0
R_{free} (%)	24.9[b]
number of protein atoms	3566
ligand molecules	2 GSBpd
other molecules	2 isopropanol
water molecules	327
rms deviations from ideal geometry	
bond distances (Å)	0.010
bond angles (deg)	1.38

[a] Crystallographic *R*-factor $= \sum_{hkl}||F_o| - |F_c||/\sum_{hkl}|F_o|$. [b] Last recorded R_{free}.

mGSTA1-1 is highly homogeneous to mGSTA2-2. Only 10 residues differ between the two isozymes, among which five are located in the last helix. However, the catalytic efficiency of mGSTA1-1 is approximately 3.3-fold higher than that of mGSTA2-2. Previous enzymatic studies on mGSTA1-1 have also shown that double mutation of 207 and 221 brings the activity of mGSTA1-1 down to that of mGSTA2-2 toward GSH conjugation of (+)-*anti*-BPDE (*22*−*24*); our crystal structure of mGSTA1-1 in complex with the GSH conjugate of (+)-*anti*-BPDE (GSBpd) suggests that R216 is also important in both substrate binding and catalysis (*25*). To elucidate the relationship between residues 207, 216, and 221 and the distinct catalytic efficiency of mGSTA1-1 and 2-2 toward (+)-*anti*-BPDE, we have determined the crystal structure of mGSTA2-2 in complex with GSBpd at 1.9 Å.

EXPERIMENTAL PROCEDURES

Crystallization and X-ray Diffraction Data Collection. mGSTA2-2 was expressed and purified as described previously (*21*, *22*). GSBpd was synthesized and purified as reported elsewhere (*20*). The hanging drop vapor diffusion technique was used to grow crystals. The drop contained 10.0 mg/mL mGSTA2-2, 5−6% PEG4000, and 3% 2-propanol in 20 mM NaHepes (pH 7.5). The molar ratio of GSBpd to protein was maintained at about 4:1. The drops were equilibrated at 15 °C against the well solution that contains 30% PEG4000, 15% 2-propanol, and 100 mM NaHepes (pH 7.5). Diffraction-quality crystals grew within a week.

X-ray diffraction data were collected at beamline X9B of the National Synchrotron Light Source at Brookhaven National Laboratory. Crystals were flash-frozen and were kept frozen at 100 K. The cryoprotectant was 0.085 M NaHepes (pH 7.5), 12.8% MPD, and 25.5% PEG4000. The crystal was annealed in the cryoprotectant for 10 min because the original test showed severe ice rings. The annealed crystal diffracted to 1.9 Å. A Quantum-4 ADSC detector was used for data collection. The raw-data images were processed and scaled using Denzo and Scalepack (*26*). Data collection statistics are summarized in Table 1.

Crystal Structure Determination and Refinement. The structure of the mGSTA2-2·GSBpd complex was solved by molecular replacement using the program AmoRe (*27*). One dimer is present in the asymmetric unit. The search model was the dimeric molecule of the crystal structure of mGSTA1-1·GSBpd (*25*) with all the water molecules removed. The rotation function was calculated using data within the resolution range of 10−4 Å and resulted in one outstanding peak with a correlation coefficient of 0.468. The result of translational search had a correlation coefficient of 0.598 and a crystallographic *R*-factor of 0.385. Rigid-body refinement within AmoRe improved the correlation coefficient and crystallographic *R*-factor to 0.705 and 0.332, respectively.

The crystal structure refinement was initiated with the CNS_0.9 package (*28*), with the maximum likelihood target function. About 5% of reflections were randomly chosen for R_{free} calculations. The starting model of mGSTA2-2·GSBpd had the uniformly assigned temperature factor of 20.0 Å^2. The first round of refinement resulted in an R_{free} of 0.355 and an *R*-factor of 0.307 for reflections of 30.0−2.0 Å with $F/\sigma(F) \geq 2$. Maps with the Fourier coefficients $2F_o - F_c$ and $F_o - F_c$ were calculated. The whole model was checked and adjusted according to the electron density maps and the primary amino acid sequence of mGSTA2-2. Residues with incomplete density were replaced with alanine or glycine. The electron density for the C-terminal helix starting from L207 to the C-terminus was poor. With the progress of refinement, water molecules were picked from the difference Fourier maps as peaks higher than 3.0 σ and were deleted if the B-factor became higher than 45 after the refinement. The data for refinement were progressively extended to 1.9 Å. Simulated-annealing omit maps were calculated to locate and verify the positions of C-terminal residues. The density of residues 207−221 was significantly improved. The GSBpd molecule was built into the difference density at 2.0 σ in the active center. The following refinement with CNS_1.0 has reduced the R_{free} and *R*-factor to 0.249 and 0.200, respectively. The final model contains 3566 protein atoms, 2 GSBpd molecules, and 327 oxygen atoms of water molecules. All X-ray diffraction data were included in electron density map calculations, and the program suite O (*29*) was used to check and modify models. A detailed summary of the crystallographic refinement is shown in Table 2.

RESULTS AND DISCUSSION

Overall Structure. The final structure has good geometry with reasonable root-mean-square (rms) deviations (Table 2). As revealed by the protein structure validation program PROCHECK (*30*), 93.1% of the residues exhibit the most

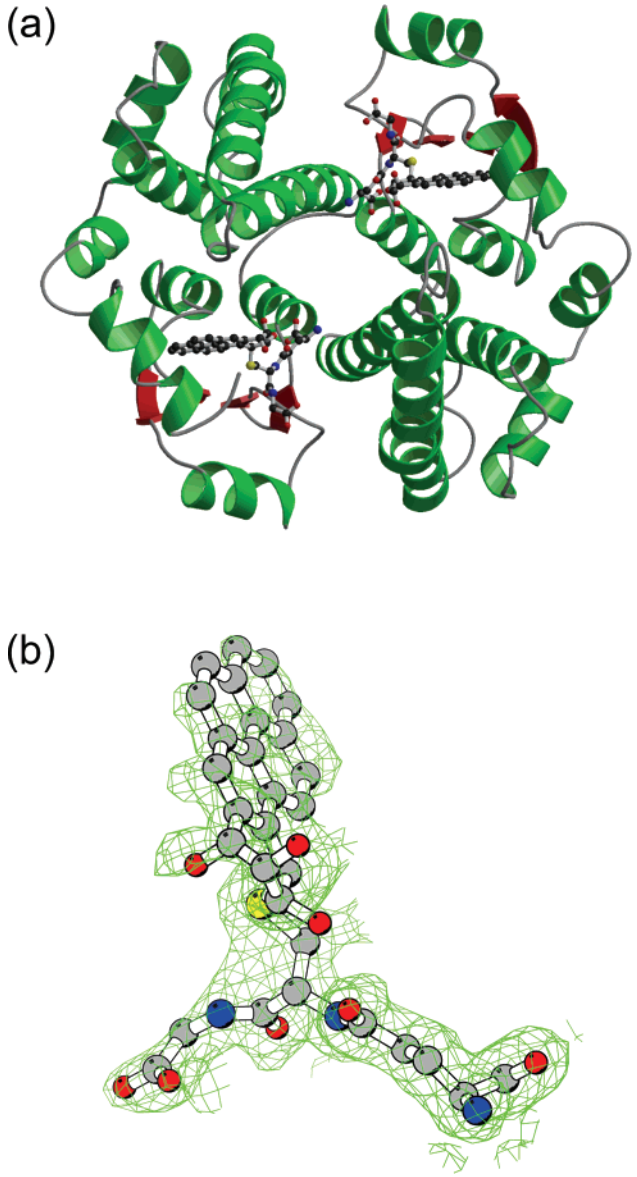

FIGURE 1: Overall structure of mGSTA2-2·GSBpd. (a) Schematic representation of dimeric mGSTA2-2·GSBpd. Green spirals are α-helices, orange arrows are β-strands, and gray tubes are loops. Ball-and-stick model with atomic color scheme (carbon, black; oxygen, red; nitrogen, blue; and sulfur, yellow) represents GSBpd, the GSH conjugate of (+)-*anti*-BPDE. (b) Final $2F_o - F_c$ electron density (green net, contour level 1.0σ) for GSBpd, which is shown as a ball-and-stick model with the atomic color scheme used in panel a with one exception: carbon is shown in gray. The figure was prepared with the program BOBSCRIPT (*33*) and Raster3D (*34*).

favorable $\phi-\varphi$ relationship, and no residue has disallowed $\phi-\varphi$ relationships. The N-terminal alanine residue in both subunits was not included because of insufficient electron density.

The overall structure of mGSTA2-2·GSBpd is schematically illustrated in Figure 1a. There is one dimer in the asymmetric unit. Each subunit is composed of nine α-helices and four β-strands, which are organized into two domains. The smaller N-terminal domain contains the secondary-structure elements β2, α1, β1, α2, β3, β4, and α3, and the larger C-terminal domain contains six α-helices (Figure 1a). The overall and domain structures are very similar to those of other class alpha GSTs, such as mGSTA1-1 (*25*) and hGSTA1-1 (*31*). The whole model has well-defined electron density. The final $2F_o - F_c$ electron density map of GSBpd molecule in the A subunit is shown in Figure 1b.

GSBpd Binding in the Active Center of mGSTA2-2. The GSBpd molecule in both subunits has the same conformation. As found in other structures of alpha class GSTs complexed with GSH or GSH conjugate, the GSH moiety of GSBpd in mGSTA2-2·GSBpd is bound to the G-site via comprehensive electrostatic interactions. Most of the polar atoms in GSH are involved in the formation of hydrogen bonds and/or salt bridges. Atom SG2 of the GSH moiety is pointing away from the OH of Y8; the distance between SG2 and atom OH of Y8 is 5.5 Å. A water molecule bridges SG2 of GSH and OH of Y8 (Figure 2a). The distance from the water oxygen to SG2/OH is 4.3/2.7 Å in subunit A and 4.1/2.6 Å in subunit B, respectively.

The hydrophobic ring system of GSBpd is located in the H-site, a hydrophobic pocket constructed by the side chains of F9, A11, L110, L207, I212, A215, R216, and F221. As depicted in Figure 2a, to the left side of the Bpd ring lie the side chains of A215 and F221, with the side chain of F221 parallel to the ring system at the average distance of 3.5−4.0 Å; on the right side of the Bpd ring are the hydrophobic side chains of L110 and L207; on the top of the Bpd ring lie the side chains of R216 and I212; and the side chains of Y8, F9, and A11 are located near the bottom of the hydrophobic Bpd moiety. Among all the active site residues that surround the Bpd moiety, Y8 and R216 have the potential of forming hydrogen bonds with the substrate. However, no hydrogen bonds are formed between Y8 or R216 and GSBpd. The −OH group of Y8 interacts with one of the hydroxyl groups of GSBpd via a water molecule, whereas the side chain of R216 lies perpendicular to the Bpd moiety, and the distance between the guanidinium group of R216 and any hydroxyl group of GSBpd is >7.5 Å (Figure 2a).

Different Binding Modes of GSBpd in mGSTA1-1 and mGSTA2-2. The overall structure of mGSTA2-2·GSBpd is very similar to that of mGSTA1-1·GSBpd. However, the conformation of GSBpd in mGSTA1-1 and mGSTA2-2 differs greatly, mainly because of the different conformation around the CB2−SG2 bond (Figure 2b). In mGSTA2-2·GSBpd, the CB2−SG2 bond is pointing away from the −OH of Y8, whereas in mGSTA1-1·GSBpd, the CB2−SG2 bond is pointing toward the hydroxyl group of Y8, forming a hydrogen bond (3.2 Å) between SG2 and −OH.

In mGSTA1-1·GSBpd, the hydrophobic ring system of GSBpd is sandwiched between the side chains of R216 and F9, with the Bpd ring system parallel to the side chains of F9 and R216 (*25*); whereas in mGSTA2-2·GSBpd, the Bpd ring system is almost perpendicular to the phenyl ring of F9 (Figure 2b). Consequently, the side chain of R216 is perpendicular to the Bpd moiety, pointing away from the active center in mGSTA2-2 (Figure 2b). Nevertheless, the stacking interaction of the Bpd ring and a phenyl ring is maintained for mGSTA2-2, of which F221 provides the phenyl ring instead of F9 (Figure 2b).

Relationship between the GSBpd-Binding Mode and GST Catalytic Activity. The two GSBpd-binding modes in mGSTA1-1·GSBpd and mGSTA2-2·GSBpd are also observed in two variants of hGSTP1-1, hGSTP1-1[V104], and hGSTP1-1[I104] (Figure 2c), where residue 104 in the H-site

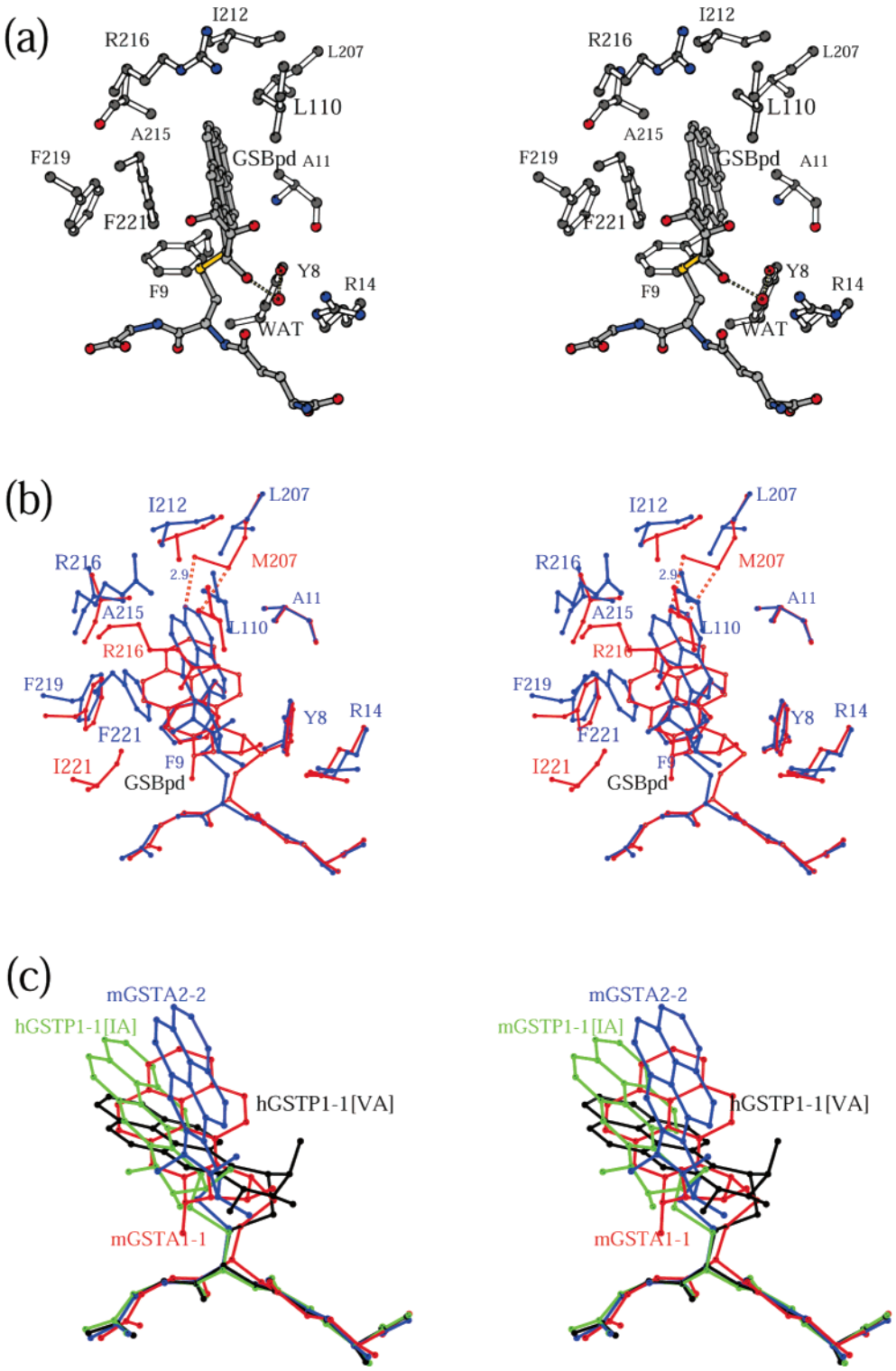

FIGURE 2: Stereoviews of the GST active center. (a) Active center architecture of mGSTA2-2·GSBpd. Ball-and-stick model is used with atomic color scheme (carbon, gray; oxygen, red; nitrogen, blue; and sulfur, yellow). Hydrogen bonds and electrostatic interactions are shown as dashed lines. (b) Active center comparison of mGSTA1-1·GSBpd (red) and mGSTA2-2·GSBpd (blue). (c) Conformational comparison of GSBpd in the crystal structures of mGSTA1-1·GSBpd (red), mGSTA2-2·GSBpd (blue), hGSTP1-1[I104,A113]·GSBpd (green), and hGSTP1-1[V104,A113]·GSBpd (black). The figure was prepared with BOBSCRIPT (*33*).

dictates the binding modes of GSBpd (*10*). In mGSTA1-1·GSBpd and hGSTP1-1[V104]·GSBpd, a hydrogen bond (3.2 Å) is formed between −OH of the catalytic tyrosine (Y8 and Y7 in mGSTA1-1 and hGSTP1-1, respectively) and SG2 of GSBpd; whereas in mGSTA2-2·GSBpd and hGSTP1-1[I104]·GSBpd, this hydrogen bond does not exist (>5.5 Å) (Figure 2 of this work, Figure 3 in ref *10*). Provided that the (+)-*anti*-BPDE molecule binds to the H-site in the same way the GSBpd molecule does, the electrophilic center of (+)-*anti*-BPDE is aligned perfectly with the sulfur atom of GSH, and the catalytic tyrosine may be able to participate in catalysis as expected, suggesting that mGSTA1-1 and hGSTP1-1[V104] have higher catalytic activity toward (+)-*anti*-BPDE than mGSTA2-2 and hGSTP1-1[I104]. It is

indeed the case. The turnover number of mGSTA1-1 is 4.5 times that of mGSTA2-2 (*22*), and the turnover number of hGSTP1-1[V104] is 3.4 times that of hGSTP1-1[I104] (*32*).

Residues 207 and 221 in mGSTA1-1 and 2-2 Are Responsible for GSBpd-Binding Mode. In the H-site of mGSTA1-1 and mGSTA2-2, two amino acid variations are present: M207/I221 in mGSTA1-1 and L207/F221 in mGSTA2-2, respectively. It appears that these two residues are responsible for the different binding modes of GSBpd. First, in both structures, the shortest distance between the Bpd moiety and residue 207 is >3.4 Å. However, this distance would become 2.9 Å if residue 207 were a methionine in mGSTA2-2 (Figure 2b). Thus, the steric interaction between the side chain of M207 and the Bpd ring system in mGSTA1-1 is likely the driving force to push the Bpd ring system down and deep into the H-site. Second, in mGSTA2-2·GSBpd, the favorable stacking interaction between the phenyl ring of F221 and the Bpd moiety of GSBpd contributes also significantly to the GSBpd-binding mode (Figure 2b). It has been shown that the M207L/I221F mutant of mGSTA1-1 has a comparable catalytic efficiency as mGSTA2-2 (*22*), probably because the mutant protein of mGSTA1-1 binds (+)-*anti*-BPDE the same way as wild-type mGSTA2-2.

R216 in mGSTA2-2 May Not Be Able to Provide Electrostatic Assistance in Catalysis. Our previous studies have shown that mGSTA1-1 is about 3.3-fold more efficient than mGSTA2-2 in catalyzing the GSH conjugation of (+)-*anti*-BPDE (*21*). We also found that R216A mutation results in a marked decrease in the formation of GSBpd for both mGSTA1-1 and 2-2. Mutation of R216 to alanine results in a 58% decrease in the catalytic efficiency of mGSTA1-1; the same mutation results in a 45% decrease in the catalytic efficiency of mGSTA2-2, suggesting that R216 contributes more in the catalysis of mGSTA1-1 (*23*). The crystallographic studies of mGSTA1-1·GSH and mGSTA1-1·GSBpd suggest that R216 plays important roles in both substrate binding and catalysis by providing electrostatic assistance in the epoxide-ring opening reaction (*25*).

The structure of mGSTA2-2·GSBpd, however, reveals a significantly different conformation of R216 such that its side chain is pointing away from the H-site, and its guanidinium group does not interact with any hydroxyl group of GSBpd (Figure 2b). Therefore, R216 cannot provide any electrostatic assistance in the epoxide-ring opening reaction catalyzed by mGSTA2-2, which may account for its relatively lower catalytic efficiency in comparison with mGSTA1-1. Indeed, the R216A mutant of mGSTA1-1 has a catalytic efficiency that is comparable to that of mGSTA2-2 (*23*).

ACKNOWLEDGMENT

We thank Dr. Hong Xia for the purification of mGSTA2-2 protein and Dr. Zbigniew Dauter for his assistance and advice during the X-ray data acquisition at synchrotron beamline X9B, Brookhaven National Laboratory.

REFERENCES

1. Sheehan, D., Meade, G., Foley, V. M., and Dowd, C. A. (2001) *Biochem. J. 360*, 1−16.
2. Dixon, D. P., Lapthorn, A., and Edwards, R. (2002) *Genome Biol. 3*, REVIEWS3004.
3. Armstrong, R. N. (1991) *Chem. Res. Toxicol. 4*, 131−140.
4. Armstrong, R. N. (1994) *Adv. Enzymol. Relat. Areas Mol. Biol. 69*, 1−44.
5. Hayes, J. D., and Pulford, D. J. (1995) *Crit. Rev. Biochem. Mol. Biol. 30*, 445−600.
6. Armstrong, R. N. (1997) *Chem. Res. Toxicol. 10*, 2−18.
7. Dirr, H., Reinemer, P., and Huber, R. (1994) *Eur. J. Biochem. 220*, 645−661.
8. Ji, X., Tordova, M., O'Donnell, R., Parsons, J. F., Hayden, J. B., Gilliland, G. L., and Zimniak, P. (1997) *Biochemistry 36*, 9690−9702.
9. Ji, X., Johnson, W. W., Sesay, M. A., Dickert, L., Prasad, S. M., Ammon, H. L., Armstrong, R. N., and Gilliland, G. L. (1994) *Biochemistry 33*, 1043−1052.
10. Ji, X., Blaszczyk, J., Xiao, B., O'Donnell, R., Hu, X., Herzog, C., Singh, S. V., and Zimniak, P. (1999) *Biochemistry 38*, 10231−10238.
11. International Agency for Research on Cancer (1973) *IARC Monograph on the Evaluation of Carcinogenic Risk of Chemicals to Man*, Vol. 3, International Agency for Research on Cancer, Lyon, France.
12. Thakker, D. R., Yagi, H., Levin, W., Wood, A. W., Conney, A. H., and Jerina, D. M. (1985) in *Bioactivation of Foreign Compounds* (Anders, M. W., Ed.) pp 177−242, Academic Press, New York.
13. Buening, M. K., Wislocki, P. G., Levin, W., Yagi, H., Thakker, D. R., Akagi, H., Koreeda, M., Jerina, D. M., and Conney, A. H. (1978) *Proc. Natl. Acad. Sci. U.S.A. 75*, 5358−5361.
14. Slaga, T. J., Bracken, W. J., Gleason, G., Levin, W., Yagi, H., Jerina, D. M., and Conney, A. H. (1979) *Cancer Res. 39*, 67−71.
15. Robertson, I. G., Jensson, H., Mannervik, B., and Jernstrom, B. (1986) *Carcinogenesis 7*, 295−299.
16. Robertson, I. G., Guthenberg, C., Mannervik, B., and Jernstrom, B. (1986) *Cancer Res. 46*, 2220−2224.
17. Jernstrom, B., Funk, M., Frank, H., Mannervik, B., and Seidel, A. (1996) *Carcinogenesis 17*, 1491−1498.
18. Sundberg, K., Widersten, M., Seidel, A., Mannervik, B., and Jernstrom, B. (1997) *Chem. Res. Toxicol. 10*, 1221−1227.
19. Hu, X., Xia, H., Srivastava, S. K., Pal, A., Awasthi, Y. C., Zimniak, P., and Singh, S. V. (1998) *Cancer Res. 58*, 5340−5343.
20. Hu, X., Srivastava, S. K., Xia, H., Awasthi, Y. C., and Singh, S. V. (1996) *J. Biol. Chem. 271*, 32684−32688.
21. Xia, H., Pan, S. S., Hu, X., Srivastava, S. K., Pal, A., and Singh, S. V. (1998) *Arch. Biochem. Biophys. 353*, 337−348.
22. Xia, H., Gu, Y., Pan, S. S., Ji, X., and Singh, S. V. (1999) *Biochemistry 38*, 9824−9830.
23. Pal, A., Gu, Y., Herzog, C., Srivastava, S. K., Zimniak, P., Ji, X., and Singh, S. V. (2001) *Carcinogenesis 22*, 1301−1305.
24. Pal, A., Gu, Y., Pan, S. S., Ji, X., and Singh, S. V. (2001) *Biochemistry 40*, 7047−7053.
25. Gu, Y., Singh, S. V., and Ji, X. (2000) *Biochemistry 39*, 12552−12557.
26. Otwinowski, Z., and Minor, W. (1997) *Methods Enzymol. 276*, 307−326.
27. Navaza, J. (1994) *Acta Crystallogr. A 50*, 157−163.
28. Brünger, A. T., and Rice, L. M. (1997) *Methods Enzymol. 277*, 243−269.
29. Jones, T. A., and Kjeldgaard, M. (1997) *Methods Enzymol. 277*, 173−208.
30. Laskowski, R. A., MacArthur, M. W., Moss, D. S., and Thornton, J. M. (1993) *J. Appl. Crystallogr. 26*, 283−291.
31. Sinning, I., Kleywegt, G. J., Cowan, S. W., Reinemer, P., Dirr, H. W., Huber, R., Gilliland, G. L., Armstrong, R. N., Ji, X., Board, P. G., Olin, B., Mannervik, B., and Jones, T. A. (1993) *J. Mol. Biol. 232*, 192−212.
32. Hu, X., O'Donnell, R., Srivastava, S. K., Xia, H., Zimniak, P., Nanduri, B., Bleicher, R. J., Awasthi, S., Awasthi, Y. C., Ji, X., and Singh, S. V. (1997) *Biochem. Biophys. Res. Commun. 235*, 424−428.
33. Kraulis, P. J. (1991) *J. Appl. Crystallogr. 24*, 946−950.
34. Merritt, E. A., and Bacon, D. J. (1997) *Methods Enzymol. 277*, 505−524.

BI026778+